Supplementary Information for

The inhibition of LSD1 via sequestration contributes to tau-mediated neurodegeneration

Amanda K. Engstrom[1], Alicia C. Walker[1], Rohitha A. Moudgal[1], Dexter A. Myrick[1], Stephanie M. Kyle[1], Yu Bai,[1] M Jordan Rowley[2], David J. Katz[1*]

[1] Department of Cell Biology, Emory University School of Medicine, Atlanta GA 30322, USA.
[2] Department of Genetics, Cell Biology, and Anatomy, University of Nebraska Medical Center, Omaha, NE 68198

*Correspondence to: David J

Email: djkatz@Emory.edu.

This PDF file includes:

Materials and Methods
Figures S1 to S11
Table S1
Legends for Movies S1 to S4
Legends for Dataset S1
References for SI Appendix

Other supplementary materials for this manuscript include the following:

Movies S1 to S4
Dataset S1
Dataset S2

www.pnas.org/cgi/doi/10.1073/pnas.2013552117

MATERIALS AND METHODS

All mouse work, including surgical procedures, were approved by and conducted in accordance with the Emory University Institutional Animal Care and Use Committee.

Animals

To generate tauopathy mice that are heterozygous for *Lsd1*, PS19 Tau P301S mice (Jackson Laboratory stock nos. 008169, generated by the Lee lab (*1*)) were crossed with mice that are heterozygous for *Lsd1* (*Lsd1*$^{\Delta/+}$). *Lsd1*$^{\Delta/+}$ mice were generated by crossing *Lsd1*$^{fl/+}$ mice, generated in the Rosenfeld lab (*2*), with *Vasa-Cre* transgenic mice(*3*). Once the deletion allele passes through the germline, *Lsd1* is heterozygous throughout the animal.

Mouse tissue fixation

Mice were given a lethal dose of isoflurane via inhalation, then transcardially perfused with ice cold 4.0% paraformaldehyde in 0.1M phosphate buffer. Brain and spinal cord were dissected and post fixed in cold paraformaldehyde solution for 2 hours. Brain weights and sizes were taken from mice that were euthanized by cervical dislocation. Brain was dissected, immediately weighed, imaged, and fixed in cold 4.0% paraformaldehyde in 0.1M phosphate buffer overnight. In all cases, tissues were transferred to cold PBS, then serially dehydrated and embedded in paraffin and serially sectioned into 8μm coronal sections.

Histology and histological studies

Hematoxylin and eosin staining was performed according to standard procedures. Briefly, sections were dewaxed with xylenes and serial ethanol dilutions then stained with Eosin using the Richard-Allan Scientific Signature Series Eosin-Y package (ThermoScientific). To derive unbiased estimates of neuronal loss in the hippocampus, the number of primordial neurons in CA1 and CA3 (corresponding approximately to bregma coordinates -2.0 mm and -3.0 mm) were

counted from 2 randomly selected regions in the field of a Zeiss Axiophot ocular graticule grid and measured manually using digital micrographs of H&E-stained preparations. Investigators were blinded to the genotype or treatment.

Immunohistochemistry and immunofluorescence

Sections were dewaxed with xylenes and serial ethanol dilutions, then treated with 3% hydrogen peroxide at 40°C for 5 minutes to quench endogenous peroxidase activity, blocked in 2% serum at 40°C for 15 minutes, and incubated with primary Ab (Table S1) overnight at 4°C. Slides were washed, then incubated with biotinylated secondary Ab (Biotinylated Goat α Rabbit, 1:200, Vector Labs BA-1000 or Biotinylated Goat α Mouse, 1:200, Vector Labs BA-9200) at 37°C for 30 minutes. Signal amplification was then carried out by incubating at 37°C for 1 hour with Vector Labs Elite ABC reagent (PK-6200). Slides were developed with DAB for 1-5 minutes, counterstained with hematoxylin for 1 minutes, and coverslipped. For immunofluorescence, dewaxed sections were first rinsed with TBS. Antigen retrieval was performed by microwaving at 10% power 2X for 5 minutes in 0.01M sodium citrate. Slides were then cooled, washed with TBS, permeabilized in 0.5% Triton X-100 for 20 minutes, followed by blocking in 10% goat serum 20 minutes. Primary Abs (Table S1) were incubated overnight at 4°C. Slides were then washed and incubated in secondary Abs (Invitrogen A1 1001 and Invitrogen A11012) for 1 hour at room temperature, followed by TBS washes, counterstained with DAPI, and then coverslipped. For the assessment of tau accumulation, six random sections (sampling from CA1, CA3, and cerebral cortex) per sample were manually counted using digital micrographs of AT8 stained preparations in the field of a Zeiss Axiophot ocular graticule grid. Investigators were blinded to the genotype or treatment. Imagining for immunofluorescence of LSD1 staining was performed on a spinning-disk confocal Nikon-Tie controlled with the software NIS Elements

(Nikon). Imaging for all other immunofluorescence staining was performed on an Eclipse Ti2 inverted microscope (Nikon, Toyko, Japan) controlled with the software NIS Elements (Nikon). Image J software ((NIH, http://imagej.nih.gov/ij/) was used for viewing all images.

Protein Quantification

Protein levels were determined by homogenizing brains in 1 ml/g of tissue in ice-cold lysis buffer (150mM NaCl, 1% Triton X-100, 0.5% Na-deoxycholate, 1% SDS, 50mM Tris, pH8.0) in a dounce homogenizer, followed by end-over-end spin at 4°C for 2 hours, and centrifugation at 20,000 x g for 20 minutes at 4°C. Protein concentrations were determined following standard BCA protocol (Pierce BCA Protein Assay Kit). Equal amounts of protein for each sample were loaded and run on a 12% SDS-PAGE gel, transferred (Semi-dry transfer using BIO RAD Trans-Blot Turbo Transfer System), blocked in 5% BSA, and probed with primary Ab (Table S1) over night at 4°C. Blots were rinsed and stained with HRP-conjugated secondary Ab, and detected by chemiluminescence using ChemiDoc MP Imaging System (BIO RAD). Protein levels were normalized using total protein calculated using BIO RAD ImageLab software.

Quantitative analysis of paralysis

We performed experiments on PS19 Tau, *Lsd1*$^{\Delta/+}$, PS19;*Lsd1*$^{\Delta/+}$ mice at 6, 8, and 10 months. For the rotarod experiments, mice were given two practice trials and then placed on the rotating cylinder at 4rpm. Rotational speed then gradually increased over a 5-minute test session up to a maximum rotational speed of 40rpm. Latency to fall off of the accelerating rotarod was used as the dependent variable. We calculated the latency to fall, maximum speed in rotations per minute, and distance traveled. For grid performance, mice were placed on a horizontal grid that was then inverted so mice are hanging upside down by their paws. Mice were videotaped for 10

seconds, and then scored for forepaw and back paw distance traveled. Mice that could not hold onto grid for 10 seconds were censored. Investigators were blinded to the genotypes for both experiments.

MRI of brain atrophy

MRI studies were conducted on PS19 Tau, *Lsd1*$^{\Delta/+}$, PS19;*Lsd1*$^{\Delta/+}$ mice at 6 months and 10 months (*n*=3/genotype). Mice were anesthetized with isoflurane, and monitored for heart rate and temperature changes while anesthetized. MRI measurements were performed using a 9.4 T/20 cm horizontal bore Bruker magnet, interfaced to an AVANCE console (Bruker, Billerica, MA, USA). A two-coil actively decoupled imaging set-up was used (a 2 cm diameter surface coil for reception and a 7.2 cm diameter volume coil for transmission). Axial T2-weighted images were acquired with a RARE (Rapid Acquisition with Refocused Echos) sequence. Its imaging parameters were as follows: TR = 3000 ms, Eff.TE = 64 ms, RARE factor = 4, field of view (FOV) = 23.04 × 23.04 mm2, matrix = 192 × 192, Avg = 4, slice thickness (thk) = 0.6 mm, number of slice(NSL)=20. Specific emphasis was placed on the neocortex and hippocampus in the coronal images (1.0 – 4.0 mm posterior to the bregma).

RNA sequencing

9 month old *Lsd1*$^{+/+}$, *Lsd1*$^{\Delta/+}$, PS19 Tau, and PS19;*Lsd1*$^{\Delta/+}$ littermates (n=2 mice/genotype) were euthanized by cervical dislocation, hippocampi were dissected and snap frozen with liquid nitrogen in 1mL Trizol, and stored at -80°C. For RNA isolation, samples were thawed at 37°C then kept on ice prior to homogenization with Polytron homogenizer with a 5 second pulse. After a 5 minute incubation at room temperature, one tenth the sample volume of 1-bromo-3chloropropane was added, mixed by inversion and incubated for 3 minutes at room temperature. Samples were then centrifuged at 13,000 X g for 15 minutes at 4°C to separate the aqueous and

organic layers. As much of the aqueous layer was recovered as possible, then RNA was precipitated with isoproponal. Pellets were then washed with 75% ethanol and resuspended in 50μL of dionized water. RNA library preparation and sequencing were performed by HudsonAlpha Genomic Services Lab. RNA was Poly(A) selected and 300bp size selected. Libraries were sequenced for 25 million 50bp paired end reads. For analysis of PS19 Tau mice injected with virus, the hippocampus was processed as above. RNA library preparation and sequencing were performed by Georgia Genomics and Bioinformatics Core. RNA was Poly(A) selected and 300bp selected. Libraries were sequenced generating ~36 million reads per sample, 75bp paired end reads.

RNA sequencing analysis

The sequencing data were uploaded to the Galaxy web platform, and we used the public server at *usegalaxy.org* to analyze the data (*4, 5*). FASTQ files were quality assessed using FASTQC (v.0.11.7), trimmed using Trimmomatic (v.0.36.5) and minimum QC score of 20 and minimum read length of 36bp. Paired-end reads were subsequently mapped to the GRCm38 genome using HISAT2 (v.2.1.0). Unmapped, unpaired and multiply mapped reads were removed using Filter SAM or BAM (v.1.1.2). Assignment of transcripts to GRCm38 genomic features was performed using Featurecounts (v.1.6.0.6) and the Ensembl GRCm38.93 gtf file. Differentially expressed transcripts were determined using DESEQ2 (v.2.11.40.2) *(5)*. For all datasets, a cutoff of adjusted p-value < 0.3 and abs ($\log_2$ fold change) > 0.58 was applied. TPM values were calculated from raw data obtained from Featurecounts output. Subsequent downstream analysis was performed using R and normalized counts and adjusted P-values from DESEQ2 (v.2.11.40.2). Heatmaps were produced and hierarchical clustering was done using the gplots package (v. 3.0.1) and normalized counts *(6)*. Volcano plots were produced using the enhanced

volcano package (v.0.99.16) and adjusted p-values *(7)*. Additionally, Gene Set Enrichment Analysis (Pre-ranked list) was performed using the online platform WebGestalt *(8-11)*. Expanded Methods for RNA sequencing analysis including all R scripts are available in Dataset S2.

Stereotaxic surgery and viral infusion

All surgical procedures were approved by and conducted in accordance with the Emory University Institutional Animal Care and Use Committee. Mice were anesthetized with isoflurane (3% induction, 1-2% maintenance) and administered the analgesic meloxicam (5 mg/kg). Using a Stoeling Quintessential Stereotaxic Injector pump and Hamilton syringe, mice were injected with either the AAV-DJ-LSD1- HA virus or the control AAV-DJ- HA virus into both hippocampi. Each virus was injected into the rostral (AP: -2.5, ML:± 2.2, DV: -1.6, relative to bregma) and caudal (AP: -3.1, ML:± 3.0, DV: -3.5) hippocampus of both hemispheres (four injection sites total). Infusion volumes were 0.5 µL per injection site, administered at a rate of 0.15 µL/min. Following surgery, mice were monitored daily for the duration of the experiment. Brains were extracted 3 months post-surgery which allows sufficient time for viral expression. Injection accuracy was confirmed by HA positive staining, and those mice where staining was outside the hippocampus or that did not fully reach hippocampus were censored.

Statistical analysis

Data are expressed as the either the mean± SD (SEM for LSD1 localization and paralysis quantification), or box-and-whisker plots where the box plot edges are 25^{th} and 75^{th} percentile, central line is the median, and whiskers are maximum and minimum. Because the data were normally distributed, parametric tests were used to analyze the data in GraphPad Prism version 7 (GraphPad software, San Diego, CA). Data were analyzed via one-way or two-way ANOVA

with post hoc Tukey's test for multiple comparisons when appropriate. The survival curve was analyzed using the Log-rank Mantle-Cox test. Significance was set at $P<0.05$ and two-tailed variants of tests were used throughout. Each specific test and number of independent experimental trials (*n*) are described in the figure legends coordinating with data shown.

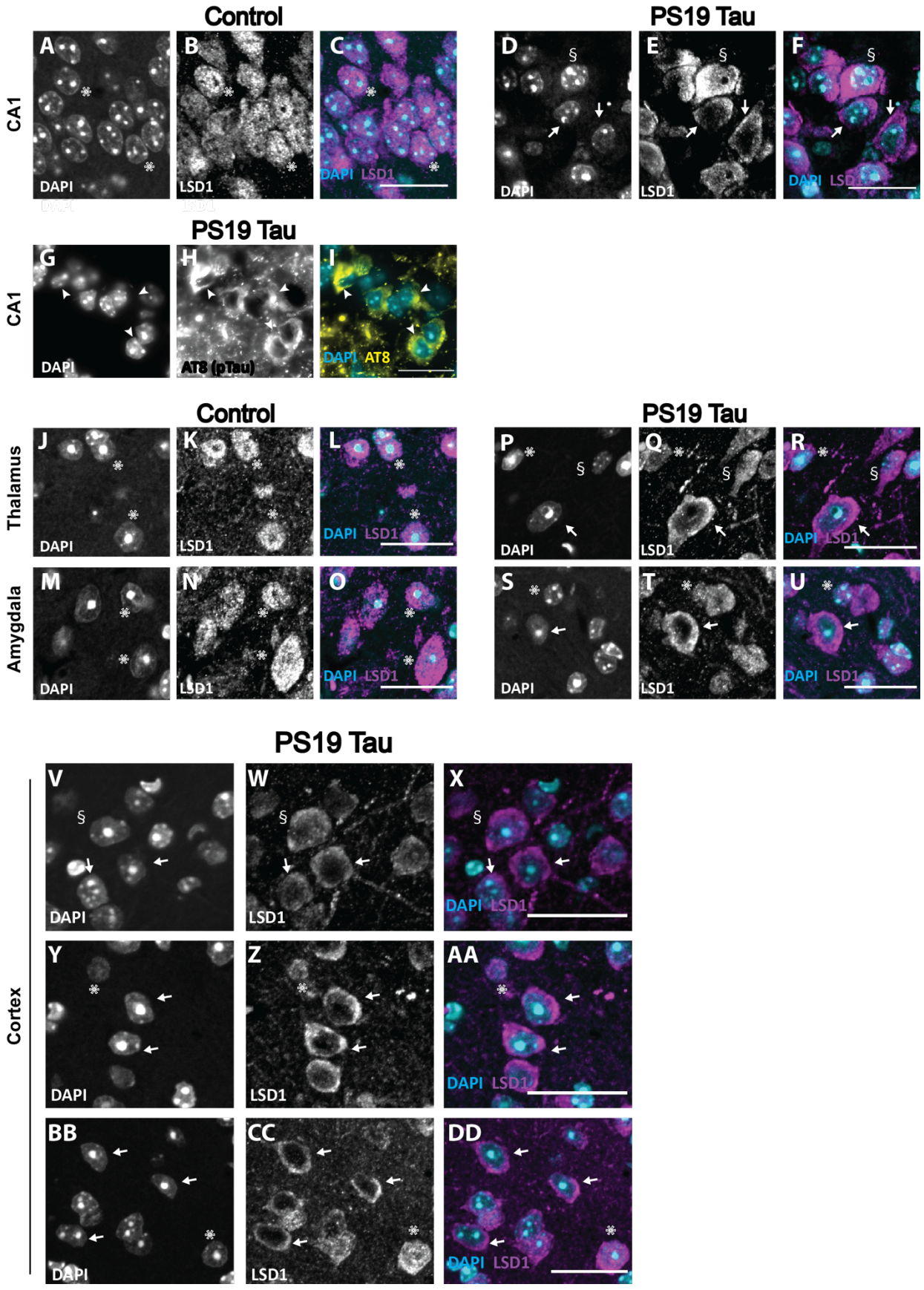
Control
PS19 Tau
CA1
A
B
C
D
E
F
DAPI
LSD1
DAPI LSD1
§
PS19 Tau
CA1
G
H
I
DAPI
AT8 (pTau)
DAPI AT8
Control
PS19 Tau
Thalamus
J
K
L
P
Q
R
Amygdala
M
N
O
S
T
U
PS19 Tau
Cortex
V
W
X
Y
Z
AA
BB
CC
DD

Fig. S1: Sequestration of LSD1 in PS19 Tau mice. A-F, Representative immunofluorescence showing DAPI (**A,D**), LSD1 (**B,E**), and merged (**C,F**) images in the CA1 region of the hippocampus in 12 month old Wild Type (**A-C**) and PS19 Tau mice (**D-F**). **G-I**, Representative immunofluorescence showing DAPI (**G**), AT8 positive hyper-phosphorylated tau (**H**), and merged (**I**) in the CA1 region of the hippocampus of 12 month old PS19 Tau mice showing hyper-phosphorylated tau accumulation in the cytoplasm of the cell bodies. Arrowheads denote hyper-phosphorylated tau. **J-U,** Representative immunofluorescence showing DAPI (**J,M,P,S**), LSD1 (**K,N,Q,T**), and merged (**L,O,R,U**) images in the thalamus (**J-L,P-R**) and amygdala (**M-O,S-U**). In 12 month old control Wild Type mice (**J-O**), LSD1 is localized specifically to the DAPI positive nuclei, but in 12 month old PS19 Tau mice (**P-U**) LSD1 is localized outside of the nucleus. **V-DD,** Additional examples of immunofluorescence showing DAPI (**V,Y,BB**), LSD1 (**W,Z,CC**), and merged (**X,AA,DD**) of the cerebral cortex of 12 month old PS19 Tau mice. Arrows denote cells where LSD1 is localized outside of the nucleus, asterisks denote LSD1 localized specifically to the nucleus, and § denotes cells where LSD1 is both nuclear and cytoplasmic. *n*=7 mice analyzed (images representative of 6 of the 7 mice analyzed). Scale bars=25μm.

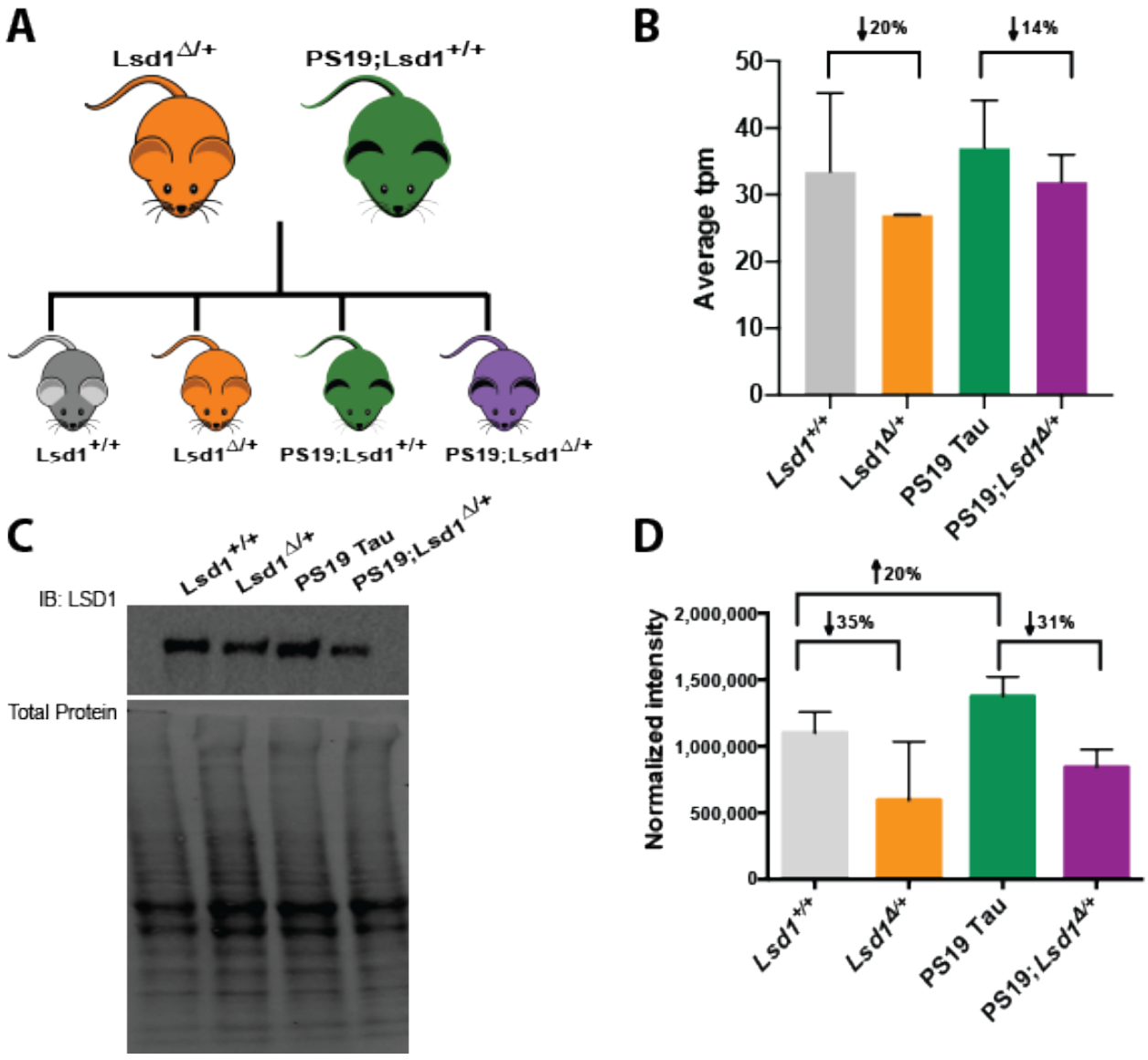

Fig. S2: Generation of PS19 Tau mice with reduced levels of LSD1. A, PS19 Tau mice carrying the P301S human tau transgene that are wild-type for *Lsd1* were crossed with *Lsd1* heterozygous mice. These crosses generated four genotypes: Wild Type mice ($Lsd1^{+/+}$, grey), *Lsd1* heterozygous mice ($Lsd1^{\Delta/+}$, orange), PS19 Tau mice that are wild-type for *Lsd1* (PS19;$Lsd1^{+/+}$ referred to as PS19 Tau, green), and PS19 Tau mice that are heterozygous for *Lsd1* (PS19;$Lsd1^{\Delta/+}$, purple). Colors designated here are maintained throughout all figures. **B,** Average transcripts per million (tpm) from RNA-sequencing of *Lsd1* expression in the hippocampus of $Lsd1^{+/+}$(*n*=4), $Lsd1^{\Delta/+}$(*n*=2), PS19 Tau (*n*=4), and PS19;$Lsd1^{\Delta/+}$ (*n*=4) mice. $Lsd1^{\Delta/+}$ mice had a 20% reduction in expression compared to $Lsd1^{+/+}$ mice, and PS19;$Lsd1^{\Delta/+}$ had a 14% reduction in expression compared to PS19 Tau mice. Values are mean ± SD, one-way analysis of variance (ANOVA) **P<0.01, ***P<0.005). **C,** Representative image of protein levels in the brain of $Lsd1^{+/+}$, $Lsd1^{\Delta/+}$, PS19 Tau, and PS19;$Lsd1^{\Delta/+}$ mice from LSD1 immunoblot and corresponding total protein blot. **D,** Quantification of immunoblot for LSD1 normalized to total protein loaded per sample as represented in **C**. Compared to $Lsd1^{+/+}$ mice, $Lsd1^{\Delta/+}$ mice had a 35% reduction and PS19 Tau mice had 20% increase in LSD1 protein levels. PS19; $Lsd1^{\Delta/+}$ mice had a 31% reduction in LSD1 protein level compared to PS19 Tau mice. Values are mean ± SD (*n*=3, one-way analysis of variance (ANOVA)).

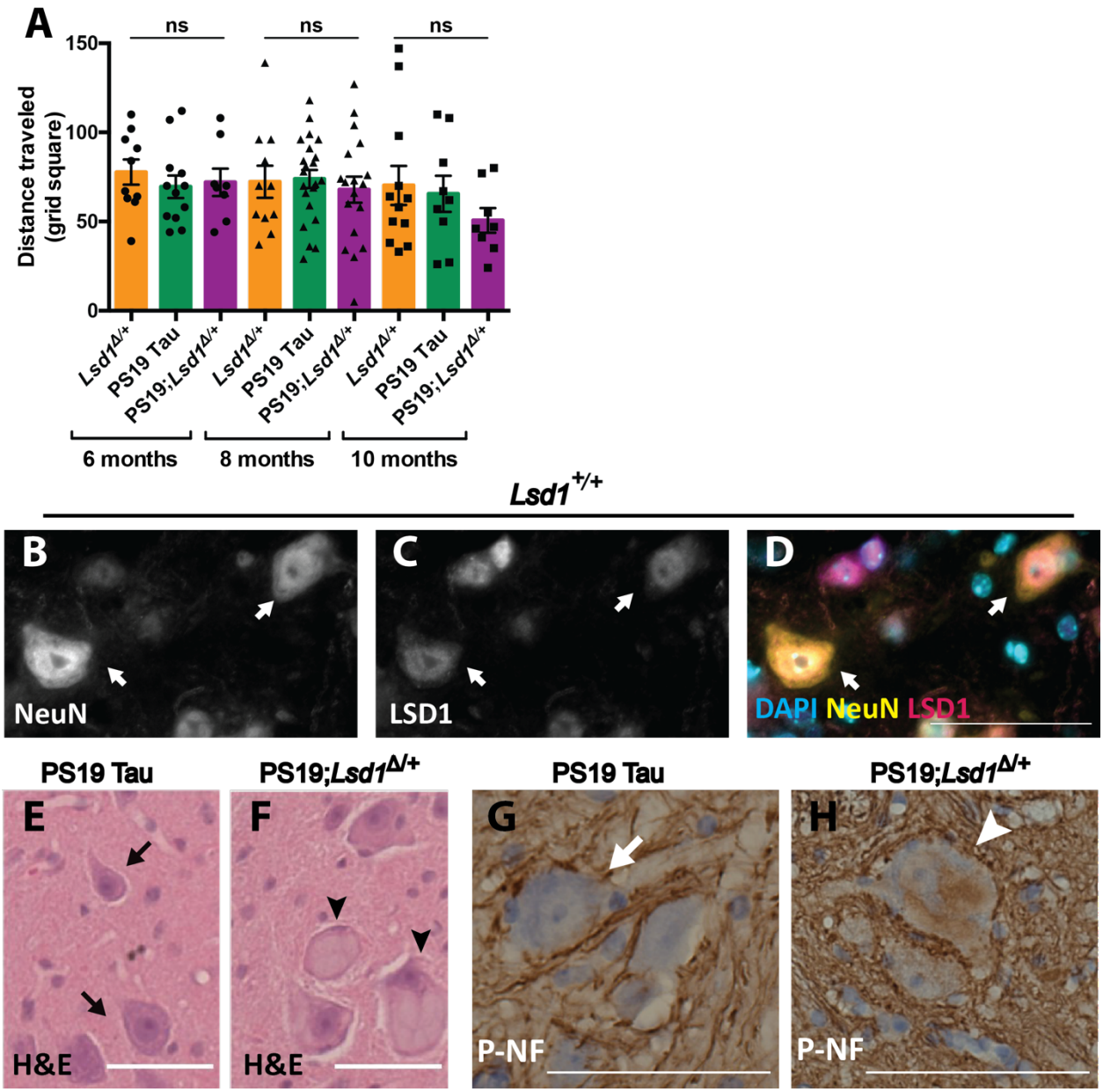

Fig. S3: Reduction of *Lsd1* affects spinal cord in PS19 Tau mice. A, Grid performance test measuring the distance traveled (grid squares traversed) with both forelimbs and hindlimbs in 6, 8, and 10 month old mice. *Lsd1*$^{\Delta/+}$ (orange, *n*=10,11,12), PS19 Tau (green, *n*=12,22,9), and PS19;*Lsd1*$^{\Delta/+}$ (purple, *n*=8,18,8). Values are mean ± SEM (two-way analysis of variance (ANOVA) with Tukey's post hoc test. ns=not significant). **B-D,** Immunofluorescence staining of NeuN (**B**), LSD1 (**C**), and merged with DAPI (**D**) in spinal cord motor neurons of 12 month old *Lsd1*$^{+/+}$ control mice. **E,F,** Representative image of hematoxylin and eosin (H&E) staining of motor neurons in 12 month old PS19 Tau mice (**E**) and PS19;*Lsd1*$^{\Delta/+}$ (**F**) littermates. **G,H** Representative image of immunohistochemistry staining for phospho-nuerofilament (brown) counterstained with DAPI (blue) in the motor neurons of 12 month old PS19 Tau mice (**G**) and PS19;*Lsd1*$^{\Delta/+}$ (**H**) littermates. Arrows denote healthy motor neurons. Arrowheads denote abnormal motor neurons. Scale bars=50μm.

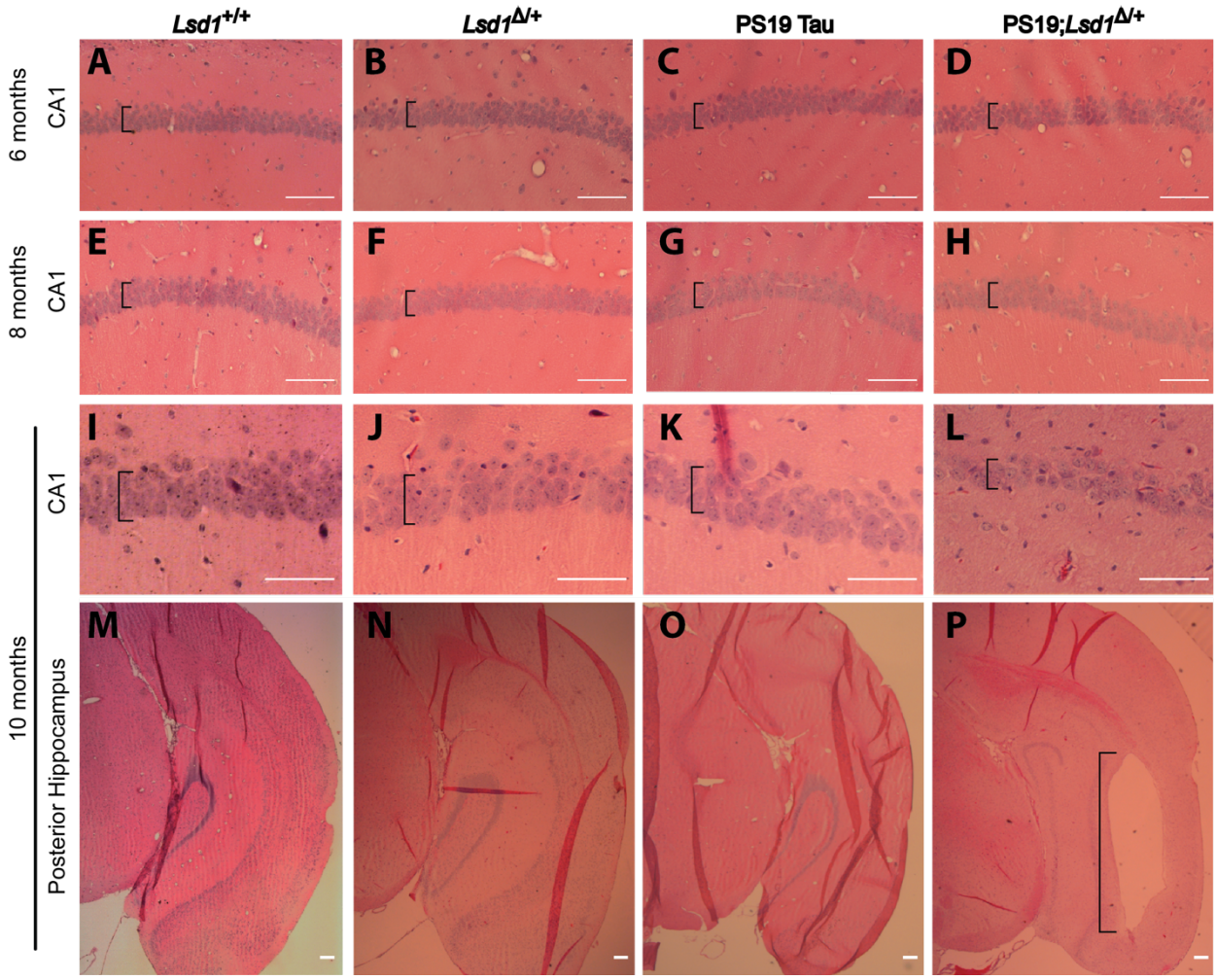

Fig. S4: There is no exacerbation of neurodegeneration in PS19 Tau mice with reduced *Lsd1* until 10 months of age. A-P, Representative image of H&E staining of *Lsd1*$^{+/+}$ (**A,E,I,M**), *Lsd1*$^{\Delta/+}$ (**B,F,J,N**), PS19 Tau (**C,G,K,O**), and PS19;*Lsd1*$^{\Delta/+}$ (**D,H,L,P**) littermates at 6 months (**A-D**), 8 months (**E-H**) and 10 months (**I-P**) in the CA1 (**A-L**) and posterior hippocampus (**M-P**). Brackets denote thickness of pyramidal layer of the CA1 (**A-L**), and region of cell clearance in posterior hippocampus (**P**). Scale bars=50μm.

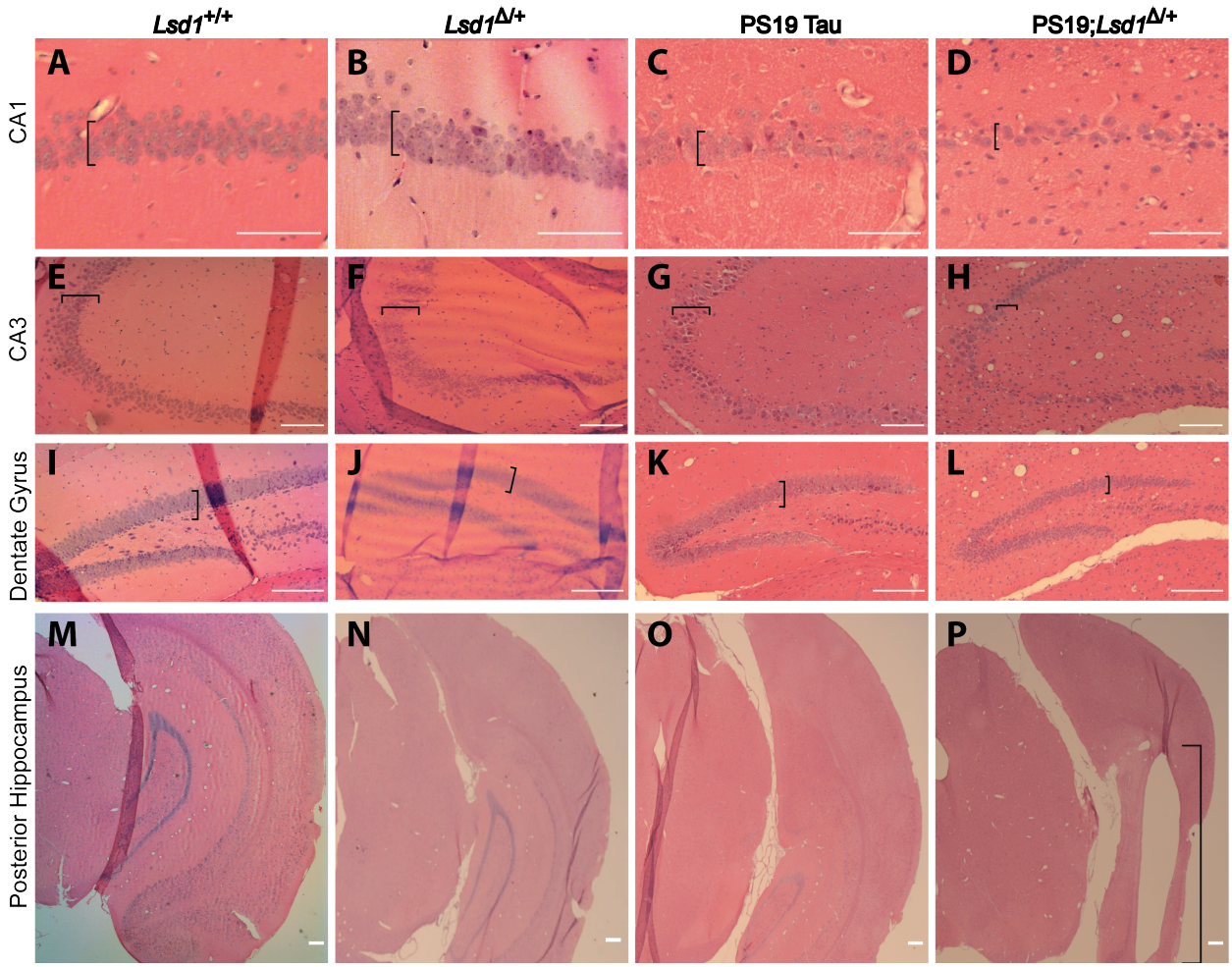

Fig. S5: Increased neurodegeneration throughout the hippocampus and cortex of 12 month old mice. A-P, H&E staining of 12 month old *Lsd1*$^{+/+}$ (**A,E,I,M**), *Lsd1*$^{\Delta/+}$ (**B,F,J,N**), PS19 Tau (**C,G,K,O**), and PS19;*Lsd1*$^{\Delta/+}$ (**D,H,L,P**) littermates in the CA1 (**A-D**) and CA3 (**E-H**) regions of the hippocampus, the dentate gyrus (**I-L**), and the posterior hippocampus (**M-P**). Brackets denote thickness of pyramidal layer of the CA1 (**A-D**), CA3 (**E-H**), the granule cell layer of the Dente Gyrus (**I-L**), and region of cell clearance in posterior hippocampus (**P**). Scale bars=50μm.

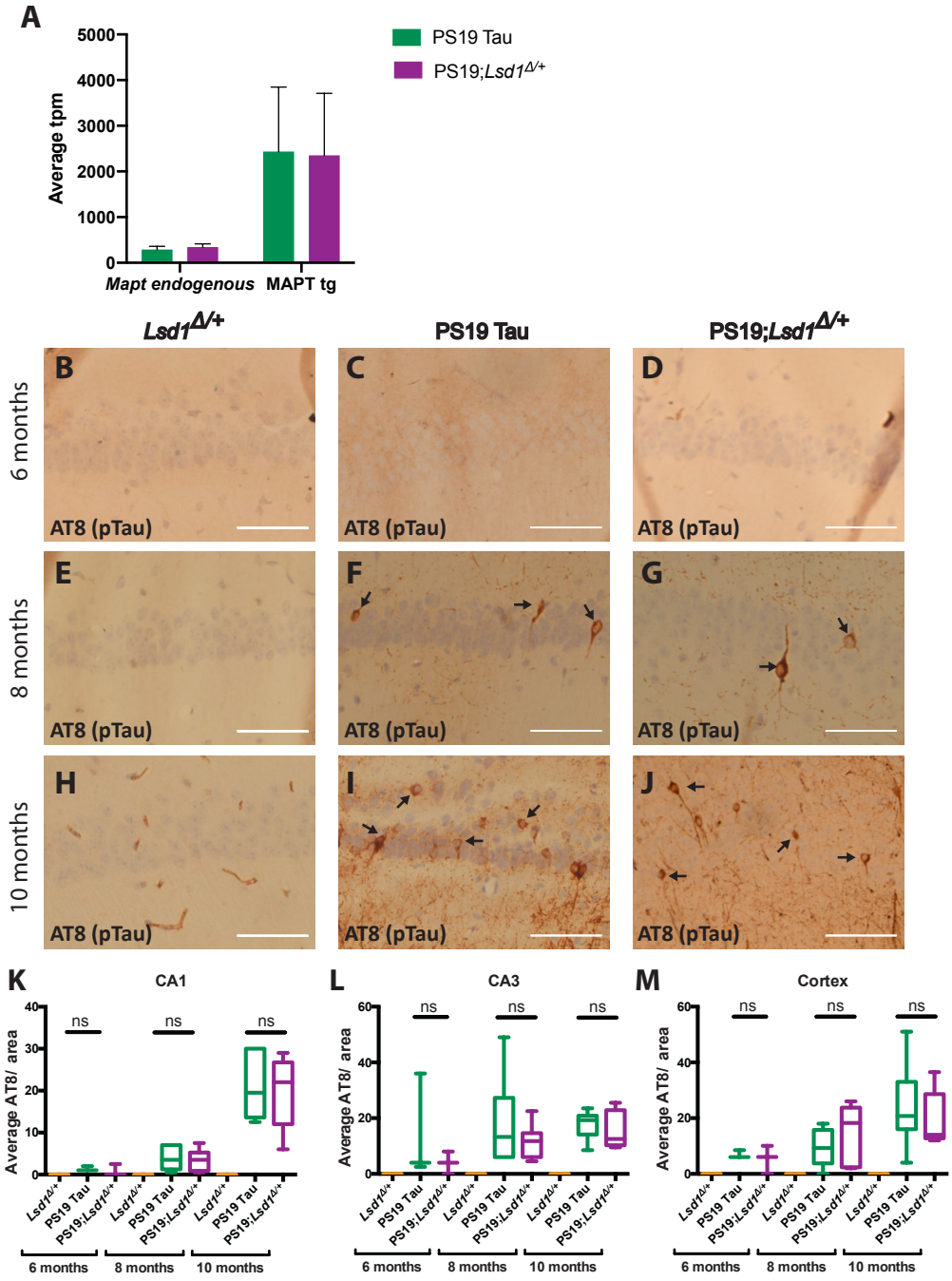

Fig. S6: Reduction of *Lsd1* does not affect AT8 positive tau pathology. A, Average transcripts per million (tpm) from RNA sequencing of endogenous *Mapt* and the expression of the human P301S MAPT transgene in the hippocampus of PS19 Tau, and PS19; *Lsd1*$^{\Delta/+}$ mice. Values are mean ± SD (*n*=4). **B-J,** Representative image of immunohistochemistry staining of phosphorylated tau (AT8 antibody) of the CA1 region of the hippocampus in *Lsd1*$^{\Delta/+}$ (**B,E,H**) , PS19 Tau (**C,F,I**), and PS19;*Lsd1*$^{\Delta/+}$ (**D,G,J**) littermates at 6 months (**B-D**), 8 months (**E-G**), and 10 months (**H-J**). Arrows denote AT8 positive immunoreactivity. Scale bars=50µm. **K-M,** Quantification of the average AT8 positive tau immunoreactivity per area from histology represented in **b-j** in the CA1 (**k**) and CA3 (**l**) regions of the hippocampus, and the cerebral cortex (**m**) (6 months *n*=3, 8 months *n*=6, and 10 months *n*=6, box plot edges are 25th and 75th percentile, central line is the median, and whiskers are max and min). For all graphs: one-way analysis of variance (ANOVA) with Tukey's post hoc test (two-sided), ns=not significant.

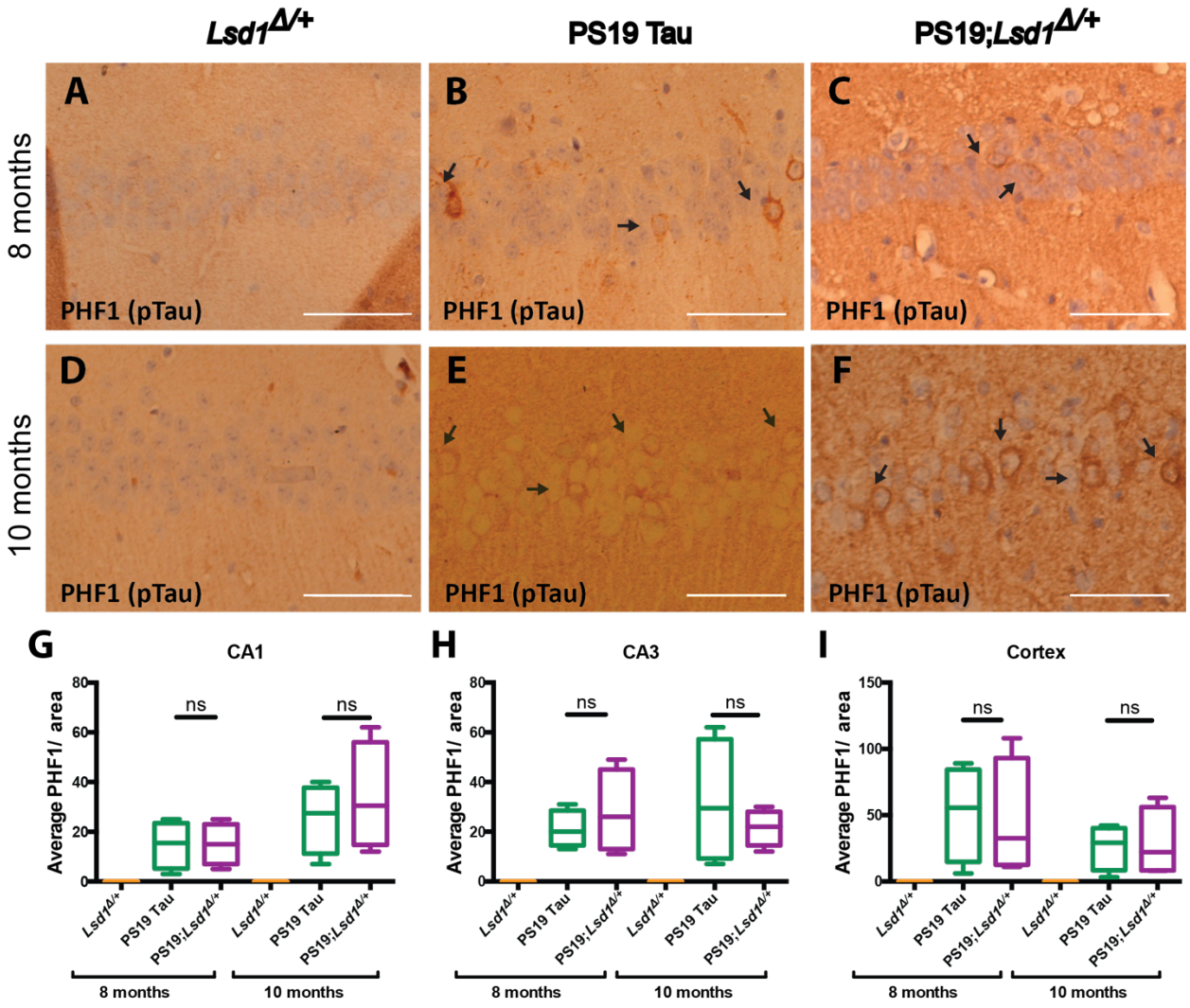

Fig. S7: Reduction of *Lsd1* does not affect PHF1 positive tau pathology. A-F, Representative image of immunohistochemistry staining of PHF1 in the CA1 region of the hippocampus in *Lsd1*$^{\Delta/+}$ (**A,D**), PS19 Tau (**B.E**), and PS19;*Lsd1*$^{\Delta/+}$ (**C,F**) littermates at 8 months (**A-C**) and 10 months (**D-F**). Arrows denote PHF1 positive immunoreactivity. Scale bars=50µm. **G-I,** Quantification of average PHF1 positive tau immunoreactivity per area from histology represented in **a-f** in the CA1 (**G**) and CA3 (**H**) regions of the hippocampus, and the cerebral cortex (**I**) (*n*=4 box plot edges are 25th and 75th percentile, central line is the median, and whiskers are max and min). For all graphs: one-way analysis of variance (ANOVA) with Tukey's post hoc test (two-sided), ns=not significant.

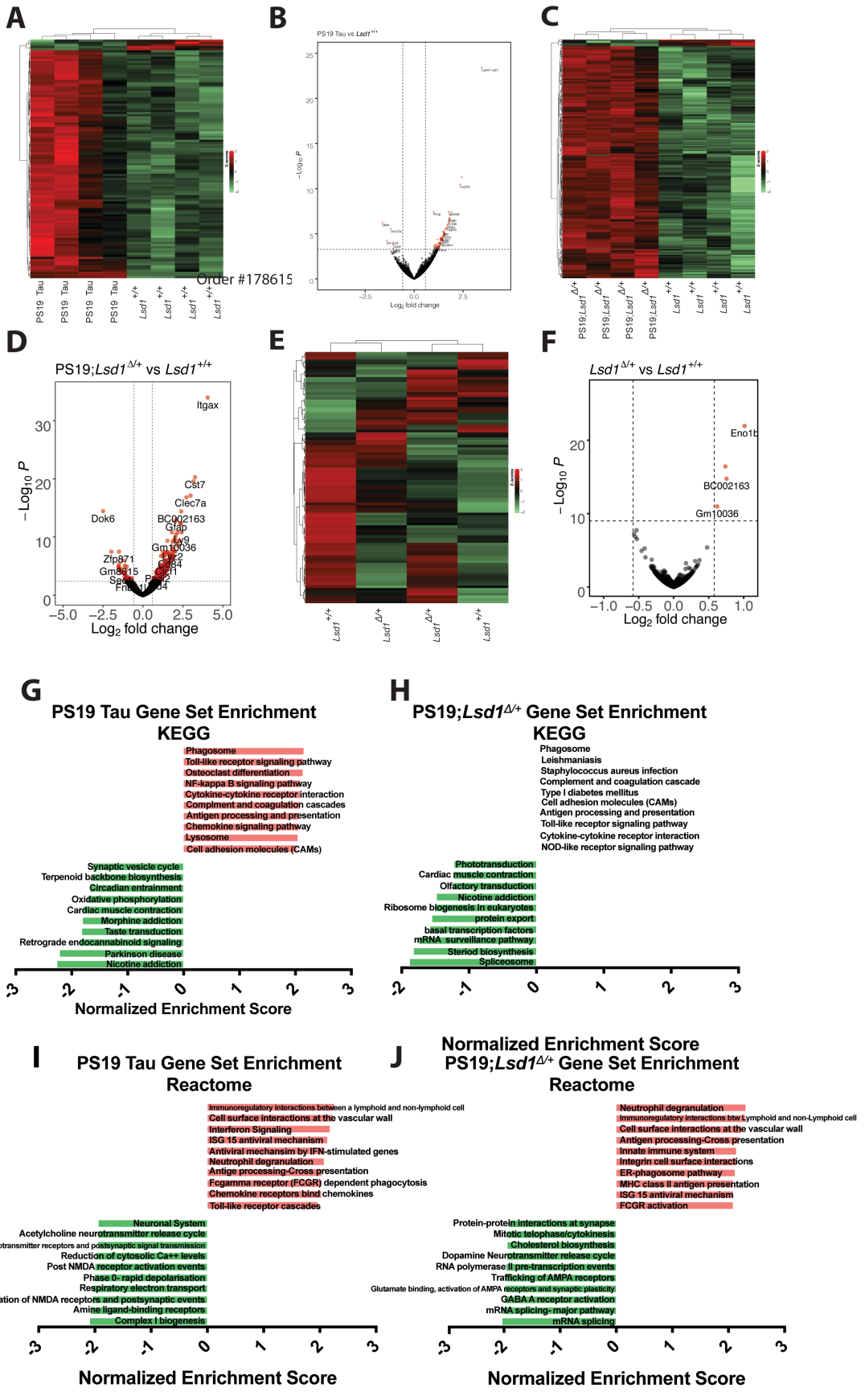
A
B
C
PS19 Tau
Lsd1 +/+
Order #178615
PS19 Tau vs Lsd1 +/+
−Log10 P
Log2 fold change
PS19;Lsd1 Δ/+
D
PS19;Lsd1 Δ/+ vs Lsd1 +/+
Itgax
Cst7
Clec7a
Dok6
BC002163
Gfap
Gm10036
Zfp871
Gm8615
E
F
Lsd1 Δ/+ vs Lsd1 +/+
Eno1b
BC002163
Gm10036
G
PS19 Tau Gene Set Enrichment
KEGG
Phagosome
Toll-like receptor signaling pathway
Osteoclast differentiation
NF-kappa B signaling pathway
Cytokine-cytokine receptor interaction
Complment and coagulation cascades
Antigen processing and presentation
Chemokine signaling pathway
Lysosome
Cell adhesion molecules (CAMs)
Synaptic vesicle cycle
Terpenoid backbone biosynthesis
Circadian entrainment
Oxidative phosphorylation
Cardiac muscle contraction
Morphine addiction
Taste transduction
Retrograde endocannabinoid signaling
Parkinson disease
Nicotine addiction
Normalized Enrichment Score
H
PS19;Lsd1Δ/+ Gene Set Enrichment
KEGG
Phagosome
Leishmaniasis
Staphylococcus aureus infection
Complement and coagulation cascade
Type I diabetes mellitus
Cell adhesion molecules (CAMs)
Antigen processing and presentation
Toll-like receptor signaling pathway
Cytokine-cytokine receptor interaction
NOD-like receptor signaling pathway
Phototransduction
Cardiac muscle contraction
Olfactory transduction
Nicotine addiction
Ribosome biogenesis in eukaryotes
protein export
basal transcription factors
mRNA surveillance pathway
Steriod biosynthesis
Spliceosome
I
PS19 Tau Gene Set Enrichment
Reactome
Immunoregulatory interactions between a lymphoid and non-lymphoid cell
Cell surface interactions at the vascular wall
Interferon Signaling
ISG 15 antiviral mechanism
Antiviral mechanism by IFN-stimulated genes
Neutrophil degranulation
Antige processing-Cross presentation
Fcgamma receptor (FCGR) dependent phagocytosis
Chemokine receptors bind chemokines
Toll-like receptor cascades
Neuronal System
Acetylcholine neurotransmitter release cycle
Neurotransmitter receptors and postsynaptic signal transmission
Reduction of cytosolic Ca++ levels
Post NMDA receptor activation events
Phase 0- rapid depolarisation
Respiratory electron transport
Activation of NMDA receptors and postsynaptic events
Amine ligand-binding receptors
Complex I biogenesis
Normalized Enrichment Score
J
Normalized Enrichment Score
PS19;Lsd1Δ/+ Gene Set Enrichment
Reactome
Neutrophil degranulation
Immunoregulatory interactions btw Lymphoid and non-Lymphoid cell
Cell surface interactions at the vascular wall
Antigen processing-Cross presentation
Innate immune system
Integrin cell surface interactions
ER-phagosome pathway
MHC class II antigen presentation
ISG 15 antiviral mechanism
FCGR activation
Protein-protein interactions at synapse
Mitotic telophase/cytokinesis
Cholesterol biosynthesis
Dopamine Neurotransmitter release cycle
RNA polymerase II pre-transcription events
Trafficking of AMPA receptors
Glutamate binding, activation of AMPA receptors and synaptic plasticity
GABA A receptor activation
mRNA splicing- major pathway
mRNA splicing
Normalized Enrichment Score

Fig. S8: Differential expression in 9 month old *Lsd1*$^{\Delta/+}$, PS19 Tau, and PS19;*Lsd1*$^{\Delta/+}$ hippocampus. A,C,E, Heatmap of differentially expressed RNA-seq transcripts between *Lsd1*$^{+/+}$ (*n*=4) and PS19 Tau (*n*=4) (**A**), PS19; *Lsd1*$^{\Delta/+}$ (*n*=4) (**C**), and *Lsd1*$^{\Delta/+}$ (*n*=2) (**E**) mouse hippocampus. Samples are hierarchically clustered by relative expression of differentially expressed transcripts. Relative higher (red) and lower (green) expression is indicated. **B,D,F,** Volcano plot of $\log_2$ fold-changes in gene expression (x-axis) by statistical significance ($-\text{Log}_{10}$ P-value; y-axis) in PS19 Tau (**B**), PS19; *Lsd1*$^{\Delta/+}$ (**D**), and *Lsd1*$^{\Delta/+}$ (**F**) compared to *Lsd1*$^{+/+}$ mouse hippocampus. Each dot represents a transcript, and the dotted line represents a significance $\log_2$ fold change cut off of 0.5. **G-J,** Histogram of Gene Set Enrichment Analysis compared to KEGG pathways (**G,H**) and the Reactome (**I,J).** The top ten most enriched (red) and depleted (green) gene sets in the PS19 Tau (**G,I**) and PS19; *Lsd1*$^{\Delta/+}$ (**H,J**) are shown with normalized enrichment scores.

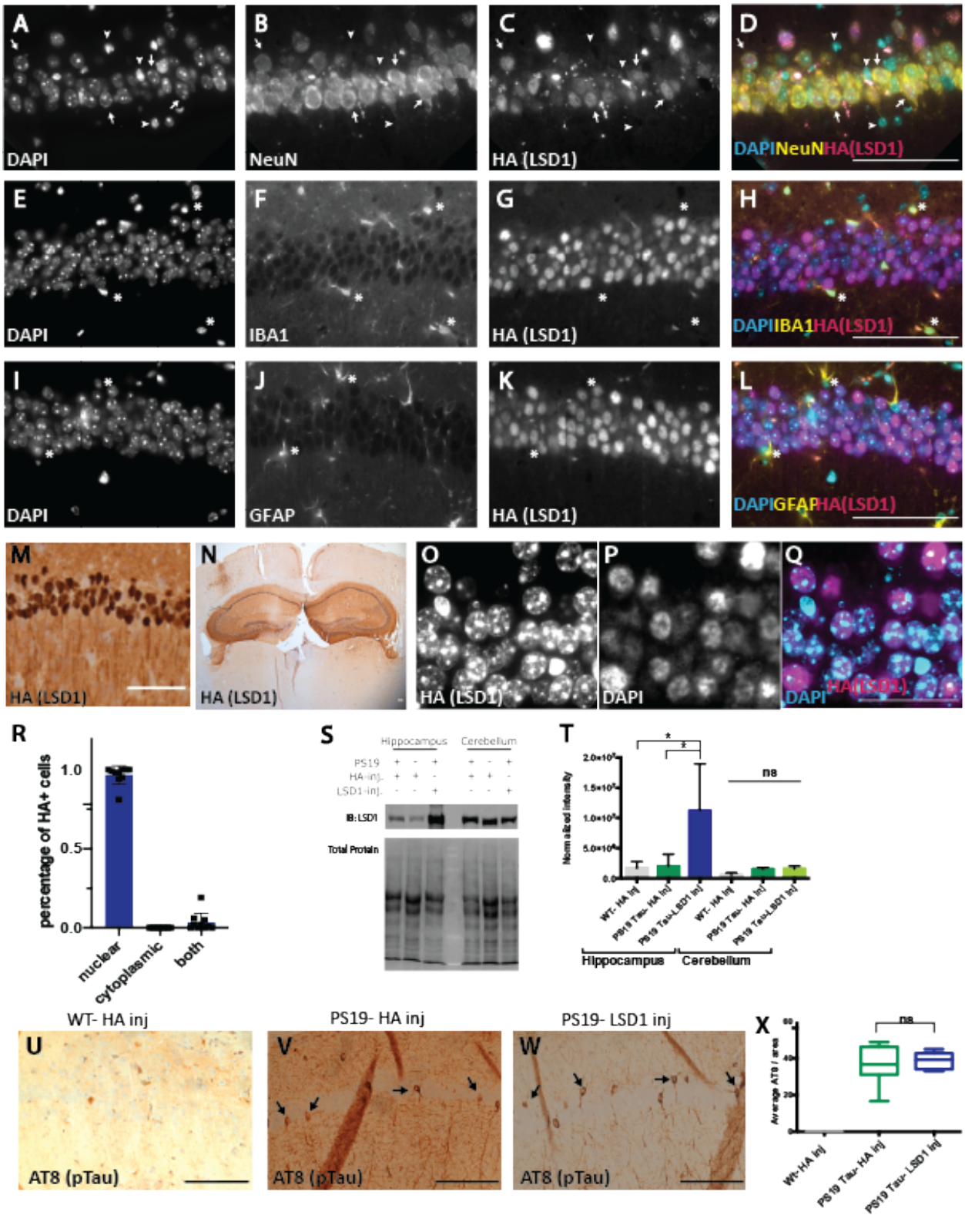
A
DAPI
B
NeuN
C
HA (LSD1)
D
DAPINeuNHA(LSD1)
E
DAPI
F
IBA1
G
HA (LSD1)
H
DAPIIBA1HA(LSD1)
I
DAPI
J
GFAP
K
HA (LSD1)
L
DAPIGFAPHA(LSD1)
M
HA (LSD1)
N
HA (LSD1)
O
HA (LSD1)
P
DAPI
Q
DAPI HA(LSD1)
R
percentage of HA+ cells
1.0
0.5
0.0
nuclear
cytoplasmic
both
S
Hippocampus
Cerebellum
PS19
HA-inj.
LSD1-inj.
IB: LSD1
Total Protein
T
Normalized intensity
2.0×10⁵
1.5×10⁵
1.0×10⁵
5.0×10⁴
0.0
*
*
ns
WT- HA inj
PS19 Tau- HA inj
PS19 Tau-LSD1 inj
WT- HA inj
PS19 Tau- HA inj
PS19 Tau-LSD1 inj
Hippocampus
Cerebellum
WT- HA inj
PS19- HA inj
PS19- LSD1 inj
U
AT8 (pTau)
V
AT8 (pTau)
W
AT8 (pTau)
X
ns
Average AT8 / area
60
40
20
0
WT-HA inj
PS19 Tau- HA inj
PS19 Tau- LSD1 inj

Fig. S9: LSD1 overexpression in hippocampal neurons of PS19 Tau mice. A-D, Representative immunofluorescence labeling in a WT- HA inj mouse showing DAPI (**A**), NeuN (**b**B, HA (which represents the LSD1 virus, hereafter denoted as HA(LSD1)) (**C**), and merged (**D**). Viral produced LSD1 is present in NeuN+ neurons. Arrows denote NeuN+ cells that have HA expression. Arrowheads denote cells that lack NeuN staining and also lack HA expression. **E-H,** Representative immunofluorescence labeling showing DAPI (**E**), IBA1 (**F**), HA(LSD1) (**G**), and merged (**H**). Asterisks denote cells stained positive for IBA1 (**E-H**), which lack HA expression. **I-L,** Representative immunofluorescence labeling showing DAPI (**I**), GFAP (**J**), HA(LSD1) (**K**), and merged (**L**) images. Asterisks denote cells stained positive for GFAP (**I-L**), which lack HA expression. **M-N,** Immunohistochemistry staining for HA(LSD1) showing expression localized to the nucleus of neurons (**M**) specifically within the hippocampus (**N**). Scale bars=50μm. **O-Q,** Representative immunofluorescence labeling of HA tagged LSD1 in 11 month old PS19-LSD1 inj mouse. DAPI (**O**), HA (LSD1) (**P**), and merged (**Q**) showing that viral produced LSD1 continues to be expressed and localized to the nucleus at the time of rescue, when LSD1 is normally becoming sequestered to the cytoplasm. Scale bars=25μm. **R,** quantification of HA(LSD1) localization shown in **O-Q.** HA (LSD1) was scored as being localized to the nucleus, the cytoplasm, or both areas. Values are mean ± SD, (*n*=10) one-way analysis of variance (ANOVA) with Tukey's post hoc test *P<0.05, **P<0.01,****P<0.001. **S,** Representative image of immunoblot for LSD1 protein and corresponding total protein blot in the hippocampus versus the cortex of mice injected with either LSD1 or HA only expressing virus. **T,** Quantification of immunoblot for LSD1 normalized to total protein loaded per sample shows overexpression in the hippocampus, but not the cortex. Values are mean ± SD (*n*=3, one-way analysis of variance (ANOVA) with Tukey's post hoc test (two-sided), *P<0.05, ns=not significant. **U-W,** Representative image of immunohistochemistry staining of phosphorylated tau (AT8 antibody) in the CA1 region of the hippocampus in 11 month old WT- HA inj (**U**), PS19- HA inj **(V),** and PS19- LSD1inj (**W**) mice. Arrows denote AT8 positive immunoreactivity. Scale bars=50μm. (**X**) Quantification of average AT8 positive tau immunoreactivity per area from histology represented in **U-W**. Box plot edges are 25th and 75th percentile, central line is the median, and whiskers are max and min (*n*=8, one-way analysis of variance (ANOVA) with Tukey's post hoc test (two-sided), ns=not significant).

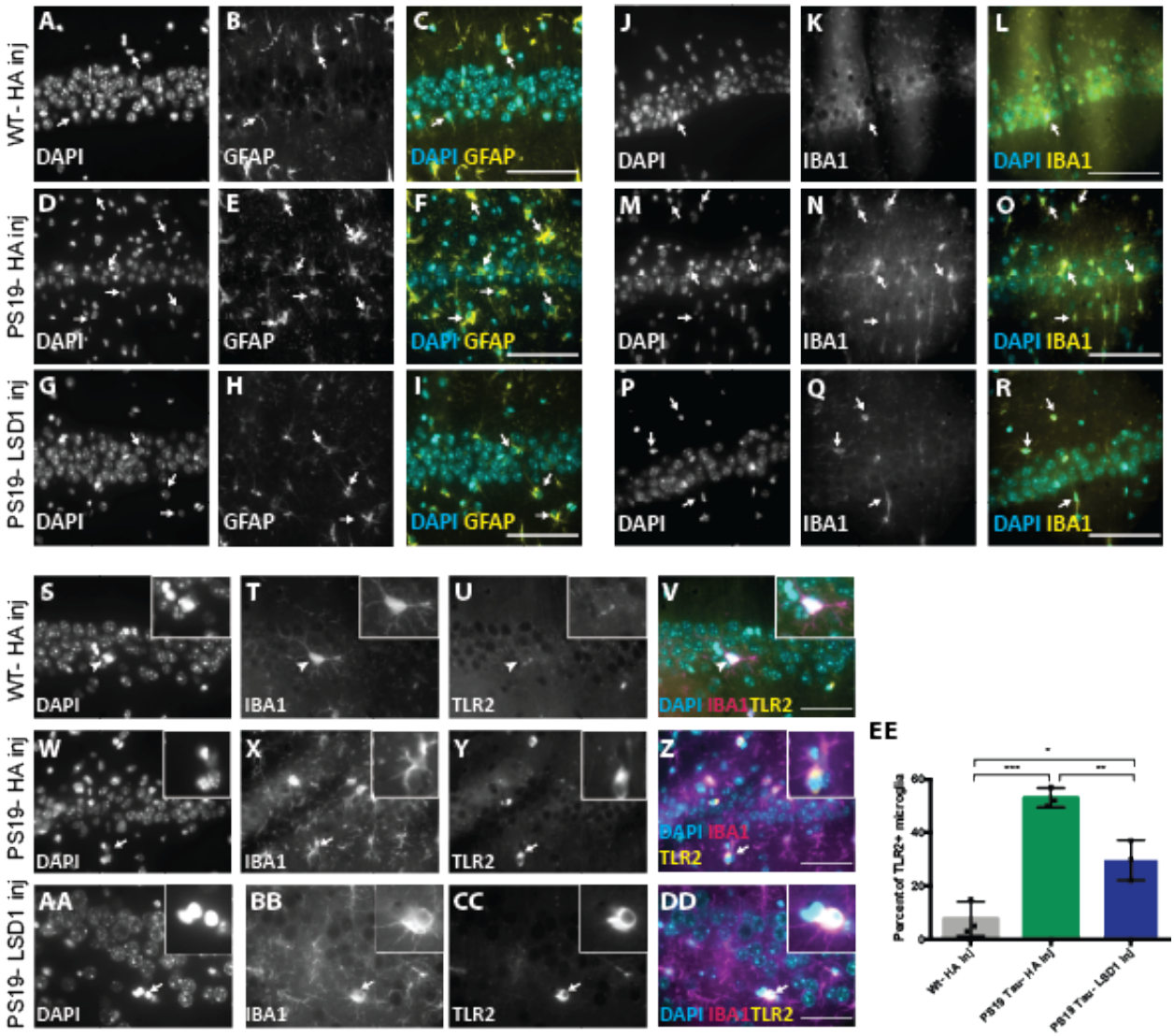

Fig. S10: LSD1 overexpression reduces the gliosis in PS19 Tau mice. A-I, Representative immunofluorescence showing DAPI (**A,D,G**), astrocyte marker GFAP (**B,E,H**), and merged (**C,D,I**) images in WT- HA inj (**A-C**), PS19-HA inj (**D-F**), and PS19- LSD1 inj (**G-I**). Arrows denote GFAP+ astrocytes. **J-R,** Representative immunofluorescence showing DAPI (**J,M,P**), microglia marker IBA1 (**K,N,Q**), and merged (**L,O,R**) images in WT-HA inj (**J-L**), PS19-HA inj (**M-N**), and PS19- LSD1 inj (**P-R**). Arrows denote IBA1+ microglia. **S-DD,** Representative immunofluorescence labeling showing DAPI (**S,W,AA**), microglia marker IBA1 (**T,X,BB**), activated microglia marker TRL2 (**U,Y,CC**), and merged (**Y,Z,DD**) images in WT-Ha inj (**S-V**), PS19-HA inj (**W-Z**), and PS19-LSD1 inj (**AA-DD**). Inset of microglia that is IBA1 positive but TRL2 negative (**S-V,** denoted by arrowhead) or both IBA1 and TRL2 positive (**W-DD**, denoted by arrow). All images are from the CA1 region of the hippocampus Scale bars=50µm. **EE,** Quantification of the percentage of microglia that are TRL2+ in WT- HA inj, PS19- HA inj, and PS19- LSD1 inj mice represented in **S-DD**. Values are mean ± SD are (*n*=3, one- way analysis of variance (ANOVA) with Tukey's post hoc test, *p<0.05, **p<0.01, ***p<0.005).

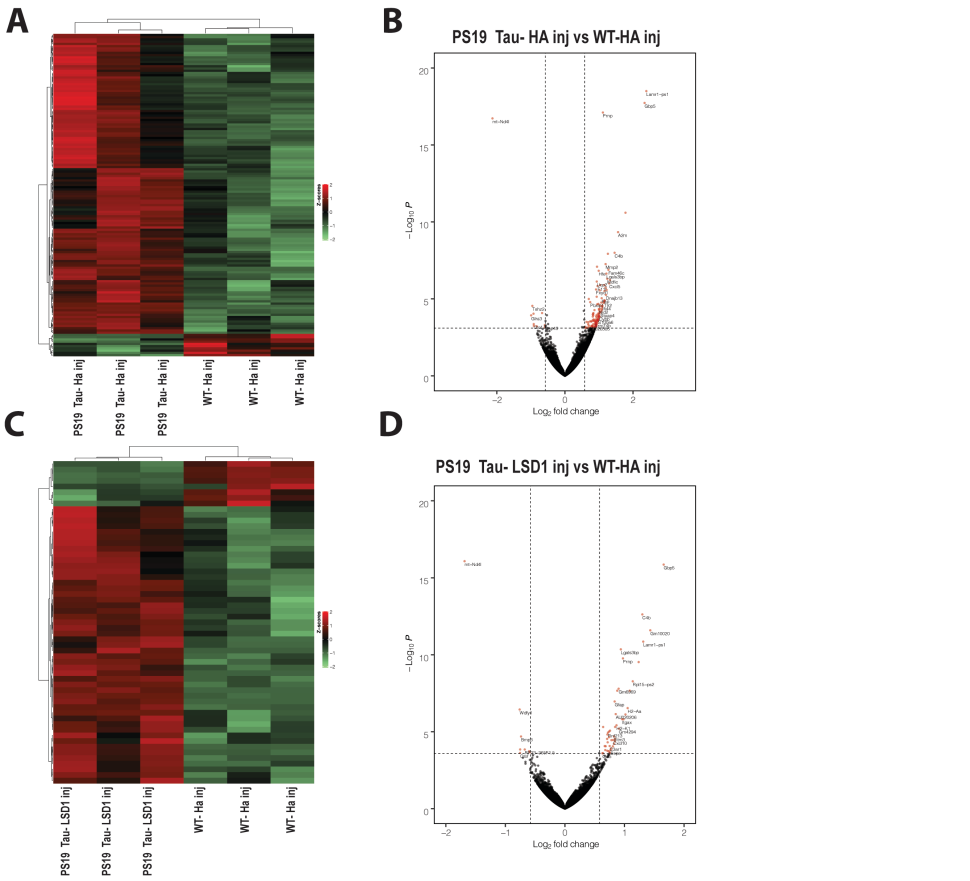
A
PS19 Tau- Ha inj
PS19 Tau- Ha inj
PS19 Tau- Ha inj
WT- Ha inj
WT- Ha inj
WT- Ha inj
B
PS19 Tau- HA inj vs WT-HA inj
−Log10 P
Log2 fold change
C
PS19 Tau- LSD1 inj
PS19 Tau- LSD1 inj
PS19 Tau- LSD1 inj
WT- Ha inj
WT- Ha inj
WT- Ha inj
D
PS19 Tau- LSD1 inj vs WT-HA inj
−Log10 P
Log2 fold change

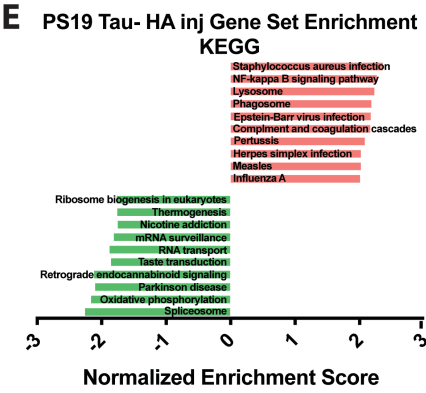
E
PS19 Tau- HA inj Gene Set Enrichment
KEGG
Staphylococcus aureus infection
NF-kappa B signaling pathway
Lysosome
Phagosome
Epstein-Barr virus infection
Complment and coagulation cascades
Pertussis
Herpes simplex infection
Measles
Influenza A
Ribosome biogenesis in eukaryotes
Thermogenesis
Nicotine addiction
mRNA surveillance
RNA transport
Taste transduction
Retrograde endocannabinoid signaling
Parkinson disease
Oxidative phosphorylation
Spliceosome
Normalized Enrichment Score

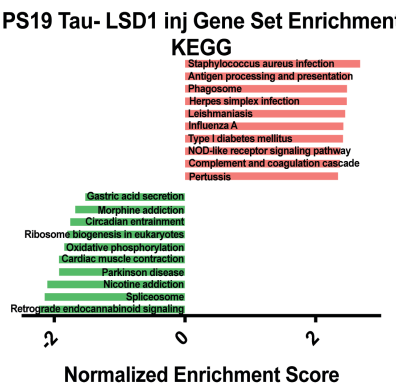
F
PS19 Tau- LSD1 inj Gene Set Enrichment
KEGG
Staphylococcus aureus infection
Antigen processing and presentation
Phagosome
Herpes simplex infection
Leishmaniasis
Influenza A
Type I diabetes mellitus
NOD-like receptor signaling pathway
Complement and coagulation cascade
Pertussis
Gastric acid secretion
Morphine addiction
Circadian entrainment
Ribosome biogenesis in eukaryotes
Oxidative phosphorylation
Cardiac muscle contraction
Parkinson disease
Nicotine addiction
Spliceosome
Retrograde endocannabinoid signaling
Normalized Enrichment Score

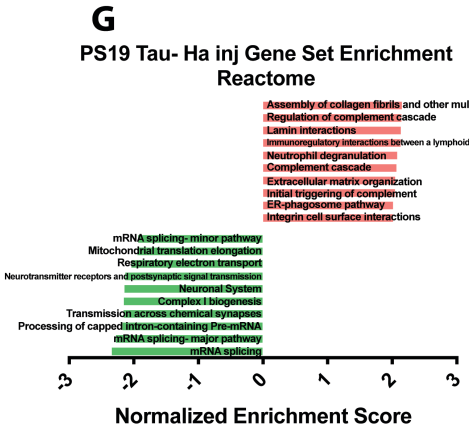
G
PS19 Tau- Ha inj Gene Set Enrichment
Reactome
Assembly of collagen fibrils and other multimeric structures
Regulation of complement cascade
Lamin interactions
Immunoregulatory interactions between a lymphoid and non-lymphoid cell
Neutrophil degranulation
Complement cascade
Extracellular matrix organization
Initial triggering of complement
ER-phagosome pathway
Integrin cell surface interactions
mRNA splicing-minor pathway
Mitochondrial translation elongation
Respiratory electron transport
Neurotransmitter receptors and postsynaptic signal transmission
Neuronal System
Complex I biogenesis
Transmission across chemical synapses
Processing of capped intron-containing Pre-mRNA
mRNA splicing-major pathway
mRNA splicing
Normalized Enrichment Score

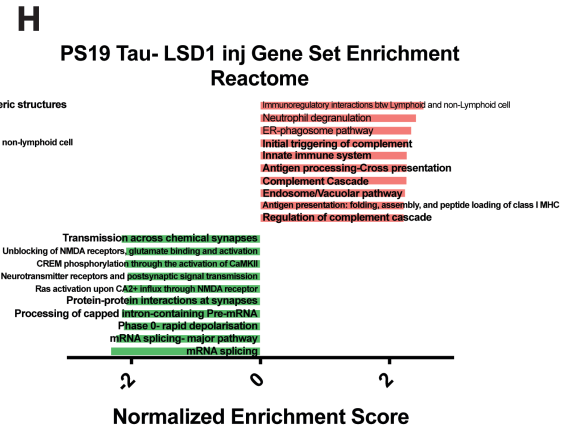
H
PS19 Tau- LSD1 inj Gene Set Enrichment
Reactome
Immunoregulatory interactions btw Lymphoid and non-Lymphoid cell
Neutrophil degranulation
ER-phagosome pathway
Initial triggering of complement
Innate immune system
Antigen processing-Cross presentation
Complement Cascade
Endosome/Vacuolar pathway
Antigen presentation: folding, assembly, and peptide loading of class I MHC
Regulation of complement cascade
Transmission across chemical synapses
Unblocking of NMDA receptors, glutamate binding and activation
CREM phosphorylation through the activation of CaMKII
Neurotransmitter receptors and postsynaptic signal transmission
Ras activation upon CA2+ influx through NMDA receptor
Protein-protein interactions at synapses
Processing of capped intron-containing Pre-mRNA
Phase 0- rapid depolarisation
mRNA splicing-major pathway
mRNA splicing
Normalized Enrichment Score

Fig. S11: Differential expression in 11 month viral injected PS19 Tau mice. A,C,, Heatmap of differentially expressed RNA-seq transcripts in PS19 Tau- HA inj (**A**) and PS19 Tau- LSD1 inj (**C**) versus WT-HA inj mouse hippocampus. Samples are hierarchically clustered by relative expression of differentially expressed transcripts. Relative higher (red) and lower (green) expression is indicated. **B,D,** Volcano plot of log_2 fold-changes in gene expression (x-axis) by statistical significance ($-Log_{10}$ P-value; y-axis) in PS19 Tau- HA inj (**B**) and PS19 Tau- LSD1 inj (**D**) compared to WT- HA inj mouse hippocampus. Each dot represents a transcript, and the dotted line represents a significance log_2 fold change cut off of 0.5. **E-H,** Histogram of Gene Set Enrichment Analysis compared to KEGG pathways (**E,F**) and the Reactome (**G,H).** The top ten most enriched (red) and depleted (green) gene sets in the PS19 Tau- HA inj (**E,G**) and PS19 Tau- LSD1 inj (**F,H)** are shown with normalized enrichment scores.

Target	Manufacturer	Clone	Lot number	Experiment	Dilution
NeuN	Millipore MAB377	A60	2392283	Mouse IF	1:500
LSD1	Abcam 17721		GR3193508-2	Mouse IF	1:100
PHF-Tau	ThermoFisher MN 1020	AT8	TI2611431	Mouse IHC	1:1,000
		AT8	TI2611431	Mouse IF	1:200
HA	Abcam ab130275	16B12	GR3190856-12	Mouse IHC	1:500
		16B12	GR3190856-12	Mouse IF	1:100
HA	Abcam ab9110		GF3224022-1	Mouse IF	1:500
GFAP	Dako Z0334		20047046	Mouse IHC	1:100
IBA1	Synaptic System 234004		2-16	Mouse IF	1:100
Neurofilament (phospho)	Millipore NE1022	SMI-31R		Mouse IHC	1:500
PHF-1	Peter Davies (Albert Einstein College of Medicine, New York, NY)			Mouse IHC	1:1,000
LSD1	Cell Signaling 2139		5	Immunoblot	1:1,000
TLR2	Abcam ab9100	TL2.1	GR3189369-7	Mouse IF	1:100

Table S1. Primary antibodies used for immunohistochemistry (IHC) and immunofluorescence (IF) experiments. Shown for each antibody are the target antigen, manufacturer, experiments used and corresponding experimental dilution.

Movie S1. Reduction of LSD1 in PS19 Tau mice exacerbates paralysis. (0-0:06 sec), Tail suspension of 12 month old *Lsd1*$^{\Delta/+}$ mouse that has full mobility in hindlimbs and no paralysis. **(0:07-0:13 sec)**, Tail suspension of 12 month old PS19 Tau mouse that has a hindlimb clasp, seen by holding legs contracted inward and not moving them, but is still mobile upon release. **(0:14-0:19 sec)**, Tail suspension of 12 month old PS19;*Lsd1*$^{\Delta/+}$ mouse that is terminally paralyzed.

Movie S2. Magnetic Resonance Imaging of hippocampal atrophy throughout the brain when LSD1 is reduced in PS19 Tau mice. (0-0:33), Serial coronal slices from T2-weighted RARE MRI, starting posterior ending anteriorly, through the brain of a 6 month old *Lsd1*$^{\Delta/+}$ mouse (**0:03-0:13**), PS19 Tau mouse (**0:13-0:22**), and PS19;*Lsd1*$^{\Delta/+}$ mouse (**0:23-0:32**). (**0:33-1:05**), Serial coronal slices from T2-weighted RARE MRI, starting posterior ending anteriorly, through the brain of the same mouse *Lsd1*$^{\Delta/+}$ mouse (**0:35-0:45**), PS19 Tau mouse (**0:45-0:55**), and PS19;*Lsd1*$^{\Delta/+}$ mouse (**0:55-1:05**) at 10 months old. High intensity areas (white/light grey) signify ventricular dilatation.

Movie S3. Hippocampal injection of viral LSD1 did not affect development of paralysis in PS19 mice. (0-0:13 sec), Tail suspension of 11 month old WT- HA inj mouse that has full mobility in hindlimbs and no paralysis. **(0:14-0:28 sec)**, Tail suspension of 11 month old PS19- HA mouse that has a hindlimb clasp, seen by holding legs contracted inward and not moving them, but is still mobile upon release. **(0:29-37sec)**, Tail suspension of 11 month old HA- LSD1 inj mouse that similarly has a hindlimb clasp holding legs contracted inward and not moving them, but is still mobile upon release.

Movie S4. Pathological Tau Induces Neurodegeneration by sequestering and inhibiting LSD1 In healthy hippocampal and cortical neurons, LSD1 is translated in the cytoplasm and transported through the nuclear pore into the nucleus where it is continuously required to repress inappropriate transcription. In tauopathy, LSD1 is translated in the cytoplasm, but as pathological tau accumulates in the cytoplasm it blocks LSD1 from being imported into the nucleus. This interferes with the continuous requirement for LSD1, resulting in neuronal cell death.

Dataset S1. (separate file)

Expression changes in 9 month old *Lsd1*$^{\Delta/+}$, PS19 Tau, PS19;*Lsd1*$^{\Delta/+}$ mice. Spreadsheets for all, significantly upregulated, and significantly downregulated transcripts. Provided for each genotype with two biological replicates are the log2 fold change, P-value, and p adjusted-value as determined by DESEQ2.

REFERENCES

1. Y. Yoshiyama *et al.*, Synapse Loss and Microglial Activation Precede Tangles in a P301S Tauopathy Mouse Model. *Neuron* **53**, 337-351.
2. Y. Jin *et al.*, Nuclear import of human histone lysine-specific demethylase LSD1. *J Biochem* **156**, 305-313 (2014).
3. T. Gallardo, L. Shirley, G. B. John, D. H. Castrillon, Generation of a germ cell-specific mouse transgenic Cre line, Vasa-Cre. *Genesis (New York, N.Y. : 2000)* **45**, 413-417 (2007).
4. E. Afgan *et al.*, The Galaxy platform for accessible, reproducible and collaborative biomedical analyses: 2016 update. *Nucleic Acids Res* **44**, W3-w10 (2016).
5. E. Afgan *et al.*, The Galaxy platform for accessible, reproducible and collaborative biomedical analyses: 2018 update. *Nucleic Acids Research* **46**, W537-W544 (2018).
6. B. B. Gregory R. Warens, Lodewijk Bonebakker, Robert Gentleman, Wolfgang Huber Andy Liaw, Thomas Lumley, Martin Maechler, Arni Magnusson, Steffen Moeller, Marc Schwartz, Bill Venables. (2019).
7. K. Blighe, in *R. package version 1.2.0*. (2019).
8. J. Wang, D. Duncan, Z. Shi, B. Zhang, WEB-based GEne SeT AnaLysis Toolkit (WebGestalt): update 2013. *Nucleic Acids Res* **41**, W77-83 (2013).
9. J. Wang, S. Vasaikar, Z. Shi, M. Greer, B. Zhang, WebGestalt 2017: a more comprehensive, powerful, flexible and interactive gene set enrichment analysis toolkit. *Nucleic Acids Res* **45**, W130-w137 (2017).
10. Y. Liao, J. Wang, E. J. Jaehnig, Z. Shi, B. Zhang, WebGestalt 2019: gene set analysis toolkit with revamped UIs and APIs. *Nucleic Acids Res* **47**, W199-w205 (2019).
11. B. Zhang, S. Kirov, J. Snoddy, WebGestalt: an integrated system for exploring gene sets in various biological contexts. *Nucleic Acids Res* **33**, W741-748 (2005).